



Electrochromism of non-stoichiometric NiO thin film: as single layer and in full device

Mathias da Rocha, Aline Rougier

► To cite this version:

Mathias da Rocha, Aline Rougier. Electrochromism of non-stoichiometric NiO thin film: as single layer and in full device. Applied physics. A, Materials science & processing, 2016, 122 (4), 10.1007/s00339-016-9923-z . hal-01327064

HAL Id: hal-01327064

<https://hal.science/hal-01327064>

Submitted on 18 Jan 2021

HAL is a multi-disciplinary open access archive for the deposit and dissemination of scientific research documents, whether they are published or not. The documents may come from teaching and research institutions in France or abroad, or from public or private research centers.

L'archive ouverte pluridisciplinaire **HAL**, est destinée au dépôt et à la diffusion de documents scientifiques de niveau recherche, publiés ou non, émanant des établissements d'enseignement et de recherche français ou étrangers, des laboratoires publics ou privés.

Electrochromism of non-stoichiometric NiO thin film: as single layer and in full device

M. Da Rocha¹ · A. Rougier¹

Abstract Electrochromic properties, known as a reversible modulation of the optical properties under an applied voltage, of NiO thin films are discussed in respect of the film stoichiometry. Using radio-frequency magnetron sputtering, non-stoichiometric “NiO” thin films of good crystallinity were grown at room temperature from low oxygen partial pressure [i.e., above 2 % P(O₂/Ar + O₂)]. A further increase in oxygen partial pressure leads to conductive brownish films containing a large amount of Ni³⁺. 2 %-Ni_{1-x}O thin films exhibit significant EC performance in lithium-based electrolyte with a transmittance modulation of 25 %. If it is generally accepted that this optical modulation is due to an insertion of small cations, the presence of additional surface phenomena is also shown. The cycling of full device, based on the association of WO₃ and “NiO” in temperature up to 60 °C and down to -35 °C confirms expected increase and decrease in capacity while surprisingly the optical switch from a transparent to a neutral gray color appears slightly modified.

1 Introduction

Electrochromism, EC, refers as a reversible phenomenon of modulation of the optical properties under an applied voltage. EC devices, ECDs, especially smart windows, have received significant attention in the past few decades,

in respect in particular of their promising application as energy saving in building due to the control of solar light transmission [1, 2]. Among materials, transition metal oxides exhibit typical electrochromism commonly illustrated by a reversible redox reaction associated with a cation insertion/deinsertion. Since the discovery of electrochromism, tungsten trioxide, WO₃ has emerged as one of the key materials and remains by far the most studied, at least among inorganic systems [3–13]. Upon reduction, transparent WO₃ thin films switch to a blue color associated with the formation of M_xWO₃, as a result of the double injection of electron and M⁺ cation, as described by the following equation:



A reversible switch to the initial transparent state is observed on the following oxidation. WO₃-based ECDs are built from the association of complementary anodically colored oxides. In order to achieve neutral color devices for commercial purposes, NiO [14–21] has widely been studied as a suitable candidate that presents the other advantage of being of lower cost than commercially used IrO_x. However, despite numerous studies, the origin of the mechanism taking place in the electrochromic behavior of NiO remains the topic of uncertainties and controversies. Among others, one reason for discrepancies results from the varieties of the synthesis methods leading to NiO thin films showing significant differences in morphology, crystallinity and stoichiometry. Focusing on the influence of the cation/oxygen ratio, non-stoichiometric NiO thin films were grown using radio-frequency magnetron sputtering technique at room temperature in various oxygen partial pressures, thereby affecting the intrinsic characteristic (morphology, initial optical transmittance, crystallinity, conductivity, etc).

✉ A. Rougier
aline.rougier@icmcb.cnrs.fr

¹ Univ. Bordeaux, ICMCB, UPR 9048, 33600 Pessac, France

One of the key issues still impeding a wide commercialization of smart windows or others ECDs is not only their durability at room temperature but the knowledge of the evolution of the EC performances in respect of high (up to 100 °C) or low temperature (−30 °C). Herein, after discussing the relationship between the film stoichiometry and the electrochromic behavior in lithium-based electrolyte, the influence of the temperature on the EC behavior of NiO-based device is reported.

2 Experimental details

Nickel oxide thin films were deposited onto ITO-coated glass substrates by reactive RF magnetron sputtering on a Leybold apparatus. The $2.5 \times 2.5 \text{ cm}^2$ glass substrates were coated with transparent conducting layers of $\text{In}_2\text{O}_3\text{:Sn}$, ITO, having a sheet resistance of $80 \text{ } \Omega/\text{sq}$. The target was 75-mm-diameter plate of metallic nickel (99.99 %), and the distance between target and substrate was 8 cm. A pre-sputtering step in argon was performed during 30 min. The $\text{P}(\text{O}_2/\text{Ar} + \text{O}_2)$ gas flow ratios (or oxygen partial pressure) varied from 0 to 10 % for a 4 Pa total pressure, and a 90 W power. The film thickness, determined by surface profilometry using a Dektak instrument, ranges from 250 nm (electrochemical measurements) to 800 nm (structural characterizations).

The film structure was determined by X-ray diffraction (XRD) using a PANalytical X'pert MPD diffractometer with CuK_α incident radiation. The morphology of the films was characterized by high-resolution scanning electron microscopy (SEM) (Hitachi Tabletop microscope TM-1000). Cyclic voltammograms, CVs, and chronoamperometry (CAs) were recorded on a Biologic potentiostat using a three-electrode glass cell consisting of glass/ITO/“NiO” as working electrode, a Pt sheet as counter electrode and a saturated calomel electrode as reference electrode [$E_{\text{SCE}} \text{ (V)} = 0.234 \text{ mV/ENH}$] and lithium-based ionic liquid electrolyte commercialized by Solvionic (purity >99.99 %), namely 0.3 M lithium bis(trifluoromethanesulfonyl)imide (LiTFSI) in 1-butyl-3-methylimidazolium bis(trifluoromethanesulfonyl)imide (BMITFSI). In situ optical transmittance measurements at 550 nm were carried on a Varian Cary UV visible NIR spectrophotometer. Experiments in temperature were performed between 60 and −35 °C. For the temperature above 25 °C, an oven was used and for the temperature below 25 °C a cryostat oil bath was used. For each experiment, the device was left at the desired temperature during 30 min before recording the CV. After the CV, the $\text{CIEL}^*a^*b^*$ colorimetric parameters were determined by Konica Minolta CM-700D spectrophotometer.

3 Results and discussion

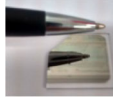
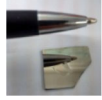


3.1 Single layer

3.1.1 Intrinsic characteristics

As a preliminary screening, the oxygen partial pressure was scanned between 0 and 10 % $\text{P}(\text{O}_2/\text{Ar} + \text{O}_2)$. Table 1 gathers some intrinsic characteristics, namely the resistance, the transmittance of the as-deposited state, the open-circuit voltage, OCV, measured in LiTFSI BMITFSI electrolyte using a three-electrode cell configuration (NiO/electrolyte/Pt vs SCE), and the visible appearance of the as-deposited state. Depending on the oxygen partial pressure, two groups of films are distinguishable showing high reflectance and low resistance or significant transmittance and high resistance. In between 0 and 0.75 % $\text{P}(\text{O}_2/\text{Ar} + \text{O}_2)$, a metallic state is observed as the amount of oxygen in the chamber appears too low to allow the formation and stabilization of an oxide. Above 2 %, an increase in oxygen partial pressure is associated with (1) a decrease in the optical transmittance from 92 % to 44 %, (2) an increase in OCV (vs SCE) value from 0.3 to 0.6 V, as well as (3) a decrease in resistance from non-measurable down to $1.6 \text{ M}\Omega$. For the 10 %-NiO thin films, additional resistivity measurements using the four-probe technique, not detailed here, conclude on a conductivity of 0.03 S cm^{-1} . Those various evolutions illustrate an increase in the Ni^{3+} content as the oxygen partial pressures increases.

While crystallizing in a cubic structure, the X-ray pattern of RT-deposited thin films evolves from nickel (SG:Fm-3m) in the case of 0 and 0.75 % to nickel oxide (SG:Fm-3m) for 2 and 10 % (Fig. 1). Whatever the oxygen partial pressure, the X-ray diffraction peaks were indexed as (1 1 1), (2 0 0) and (2 2 0), with a strong (1 1 1) preferred orientation. The crystallite size calculated using the Scherrer formula is of smaller size for Ni thin films ($\approx 15 \text{ nm}$) while it is about 35 nm for NiO thin films (Table 2). The lattice parameter of 2 % “NiO” of $4.173 \text{ } \text{\AA}$ is slightly higher than the one of bulk NiO ($4.164 \text{ } \text{\AA}$). Besides, unexpectedly in respect of smaller ionic radius of Ni^{3+} as compared to Ni^{2+} , the lattice parameter of 10 %-NiO increases to $4.191 \text{ } \text{\AA}$. Such trend in increase in cell parameter was confirmed for Ni oxide thin films deposited at even higher oxygen partial pressure. For instance, films deposited under 20 % of oxygen partial pressure exhibit a cell parameter of $4.21 \text{ } \text{\AA}$. This trend was also indeed observed by other groups [22]. However, the nature of the non-stoichiometry taking place in Ni oxide-based thin films, showing an increase in cell parameters while an increase in Ni^{3+} concentration occurs, still needs to be

Table 1 Resistance, transmittance at 550 nm and OCV measured in three electrode cell using 0.3 M LiTFSI BMITFSI electrolyte and Pt as counter electrode for 0, 0.75, 2 and 10 % “NiO” thin films of 250 nm. Visual appearance is also shown

Intrinsic characteristics	Ni		“NiO”	
	0 %	0.75 %	2 %	10 %
Resistance	5 10 Ω	5 10 Ω	Unmeasurable	1.6 M Ω
Transmittance (%) (at 550 nm)	0	0	92	44
OCV (V)	×	×	0.3	0.6
Visual appearance				

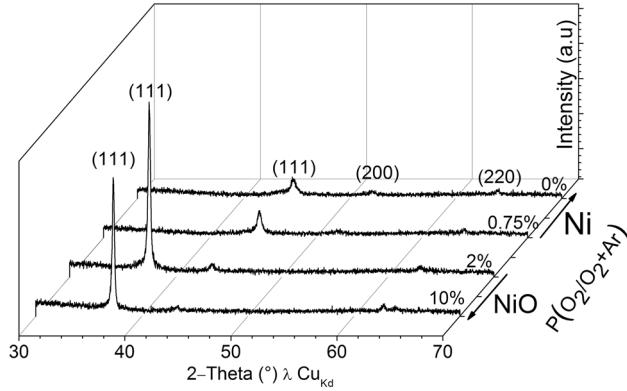


Fig. 1 X ray diffraction pattern of 800 nm 0, 0.75, 2 and 10 % NiO thin films deposited on glass substrate

Table 2 Lattice parameter and crystallite size as a function of partial pressure of oxygen for P(O₂/Ar + O₂) 0, 0.75, 2, 10 %

P(O ₂ /Ar + O ₂) (%)	Crystallite size by Scherrer (nm)	<i>a</i> (Å)
0	16	3.517 (1)
0.75	19	3.515 (1)
2	32	4.173 (1)
10	35	4.191 (1)

clarified. Using electron energy loss spectroscopy, we earlier estimated a non-stoichiometry corresponding to 17 and 30 % of Ni³⁺, for 2 %-NiO and 10 %-NiO thin films, respectively, which could be better described by the Ni_{0.92}O and Ni_{0.87}O formula [23]. In addition, the presence of OH groups, mostly associated with adsorbed water, was detected by infrared spectroscopy. The non-stoichiometry may thus be formulated as NiO(OH)_x at the film surface while Ni_{1-x}O may better describe the bulk of the film [19, 22].

As Ni thin films were electrochemically inactive, in the following, the electrochromic study is focused on Ni oxide films deposited under 2 and 10 % of oxygen partial pressure.

3.1.2 Electrochromic behavior

Figure 2 compares the CVs and the corresponding in situ transmittance at 550 nm variation, of 2 %-Ni_{1-x}O and 10 %-Ni_{1-x}O thin films cycled in Pt/0.3 M LiTFSI in BMITFSI/Ni_{1-x}O versus SCE using a 20 mV/s scan rate and -1.2 to 1.2 V voltage window. For both films, a reversible process associated with a decrease in transmittance in oxidation and an increase in reduction is observed. The larger capacity of the first reduction in the 10 %-Ni_{1-x}O ($Q_{10\%} \approx 5.7 \text{ mC/cm}^2 > Q_{2\%} \approx 1.5 \text{ mC/cm}^2$) well agrees in first approximation with the higher Ni³⁺ content,

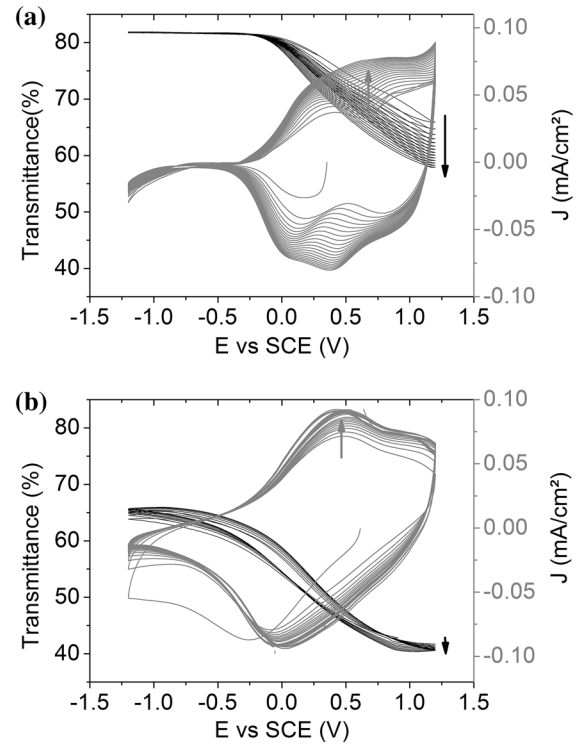
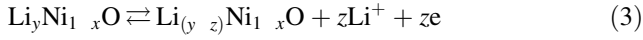


Fig. 2 a, b In situ 550 nm transmittance versus potential and CVs for 2 % Ni_{1-x}O and 10 % Ni_{1-x}O thin films cycled in Pt/0.3 M LiTFSI in BMITFSI/Ni_{1-x}O versus SCE using a 20 mV/s scan rate and -1.2 to 1.2 V voltage window

while the presence of an activation process (i.e., increase in capacity and optical modulation upon cycling) for the 2 %-Ni_{1-x}O illustrates the porous character of the films (Fig. 3).

In first approximation, the mechanism of bleaching/coloration can be schematized by a first reduction leading to the formation of Li_yNi_{1-x}O (2) followed by a reversible reaction (3):



The electrochemical capacity Q or the number of exchanged electron NEE and thus the number of exchange monovalent ions per Ni cations may be estimated using the formula:

$$Q = n(\text{NiO}) \cdot F \cdot \text{NEE} \quad (4)$$

in which n is the number of moles assuming a thin film density of 75 % and F , the Faraday constant, equal to 96,500 C. Such calculation leads to surprisingly very low values (NEE ≈ 0.009 and ≈ 0.035 for 2 %-Ni_{1-x}O and 10 %-Ni_{1-x}O) of exchanged electrons in first reduction,

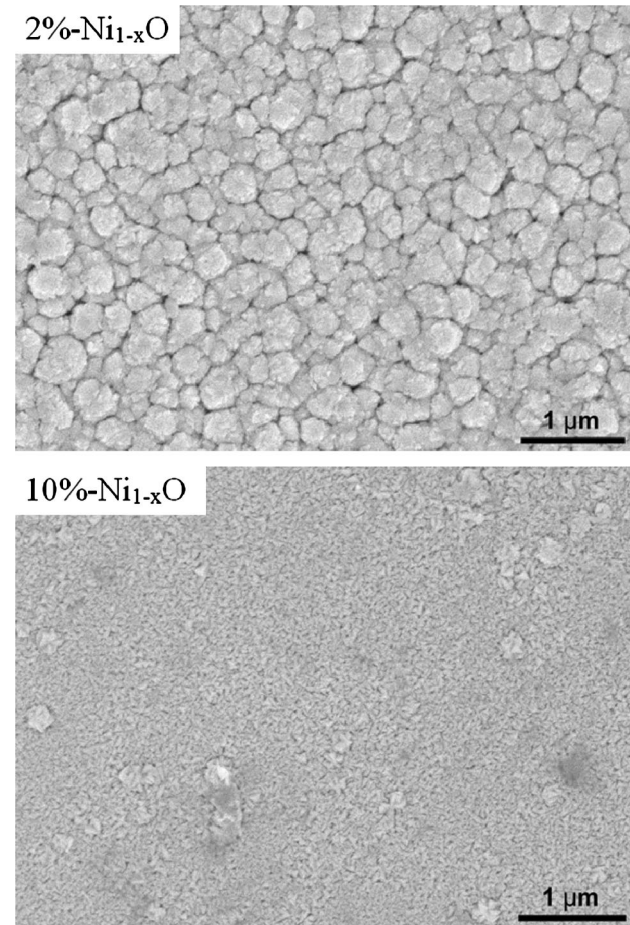


Fig. 3 SEM of 250 nm 2 %-Ni_{1-x}O and 10 %-Ni_{1-x}O thin films deposited on glass substrate

meaning that the first capacity in reduction cannot only represent a quantification of the initial Ni³⁺ content. Upon cycling a reversible capacity of NEE ≈ 0.024 is recorded for both films. Other differences, in respect of oxygen partial pressure, lie in the CV shape as well as transmittance range. For 2 %-Ni_{1-x}O, a -0.2 V potential is sufficient to reach the maximum transmittance while a lower value of 65 %, associated with remaining brownish color, requires a potential lower than -1.0 V for 10 %-Ni_{1-x}O. Overall, the transmittance modulation appears to be close to 25 % for both films corresponding to an optical contrast of 1.25 (2 %-Ni_{1-x}O) and 1.6 (10 %-Ni_{1-x}O) (the optical contrast is calculated as a ratio between the transmittance in the bleached state and in the colored state T_b/T_c). For 10 %-Ni_{1-x}O, the higher contrast is nevertheless associated with undesired lower transmittance in the bleached state, T_b ($T_{b2\%} \approx 82 \% > T_{b10\%} \approx 65 \%$). Thus, in respect of higher transmittance in the bleached state, the 2 %-Ni_{1-x}O thin films are only considered in the following. The coloration efficiency CE can be calculated using the formula:

$$\text{CE} = (1/Q) \cdot \log(T_b/T_c) \quad (5)$$

A coloration efficiency of 25 cm²/C [24] was calculated for 2 %-Ni_{1-x}O.

In first reduction, the surprising low value of NEE may suggest that the involved process is not as simple as a common insertion/deinsertion process of Li⁺. In the mean time, upon cycling, for 2 %-Ni_{1-x}O, a second anodic peak progressively appears at higher potential confirming the hypothesis that more than one process may be involved. A decrease in scan rate from 50 to 2 mV/s is associated with a progressive enlargement of the CV shape, from which was determined a couple of anodic J_{pox} and cathodic J_{pred} peaks, corresponding to the maximum of current density on anodic and cathodic scan (Fig. 4). Each value of J_{pox} was plotted against the scan rate (Fig. 5a) and square root of the

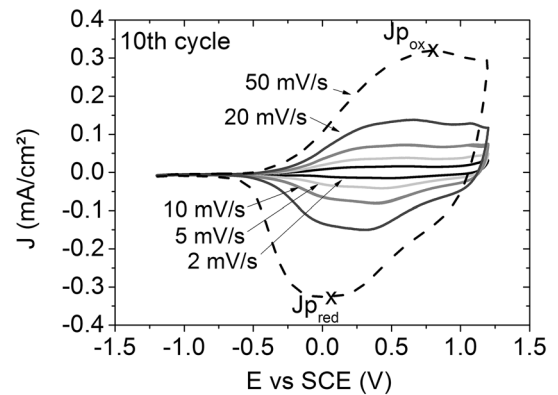


Fig. 4 CVs for 2 %-Ni_{1-x}O thin films cycled in Pt/0.3 M LiTFSI in BMITFSI/Ni_{1-x}O versus SCE using a scan rate from 2 to 50 mV/s and -1.2 to 1.2 V voltage window

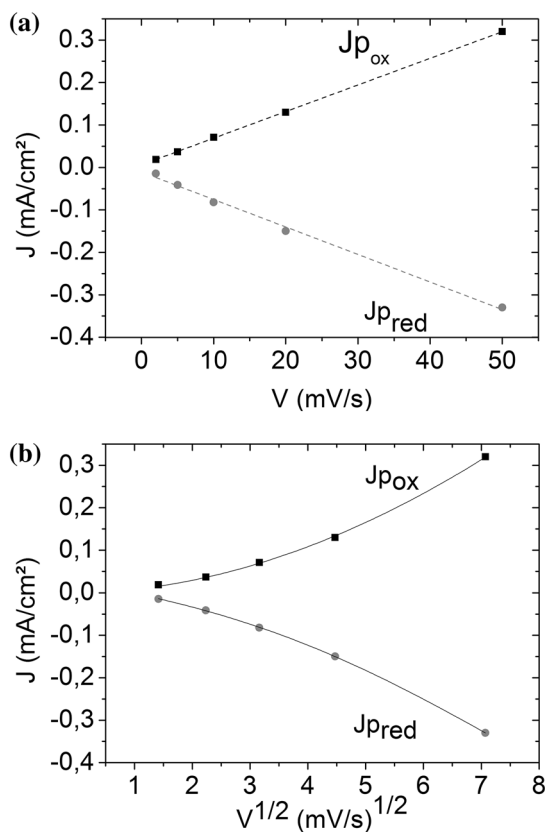


Fig. 5 Evolutions of $J_{p_{ox}}$ and $J_{p_{red}}$ of 2 % $Ni_{1-x}O$ thin films cycled in Pt/0.3 M LiTFSI in BMITFSI/ $Ni_{1-x}O$ versus SCE versus scan rate of 2 to 50 mV/s (a) and versus square root of scan rate (b)

scan rate (Fig. 5b). The linear evolution of $J_{p_{ox}}$ and $J_{p_{red}}$ versus scan rate is expected for a pseudo-capacitive behavior [25]. For further understanding, the cycling was started on oxidation. Figure 6 displays the first oxidation and CVs (2nd and 40th cycle) of 2 %- $Ni_{1-x}O$ thin film cycled in 0.3 M LiTFSI BMITFSI electrolyte with in situ measurements of the optical transmittance when started in oxidation. During the first oxidation, the transmittance decreases from 65 to 55 % suggesting an oxidation of Ni^{2+} to Ni^{3+} while no lithium was pre-inserted. Upon cycling, two couples of peaks, labeled P1 and P2, in oxidation and in reduction are clearly visible while progressively the intensity of the P2 process located at higher potential values increases. The CV's shape becomes more rectangular, and the transmittance in the colored state continues to gradually decrease on each cycle. The rectangular shape associated with the decrease in transmittance suggests that in addition of the mechanism involving Li insertion/deinsertion there is a surface phenomenon correlated with the presence/participation of TFSI⁻ anions [26]. Current investigations using various ionic liquid electrolytes confirm that upon cycling of non-stoichiometric NiO thin films not only cations but anions are involved [23].

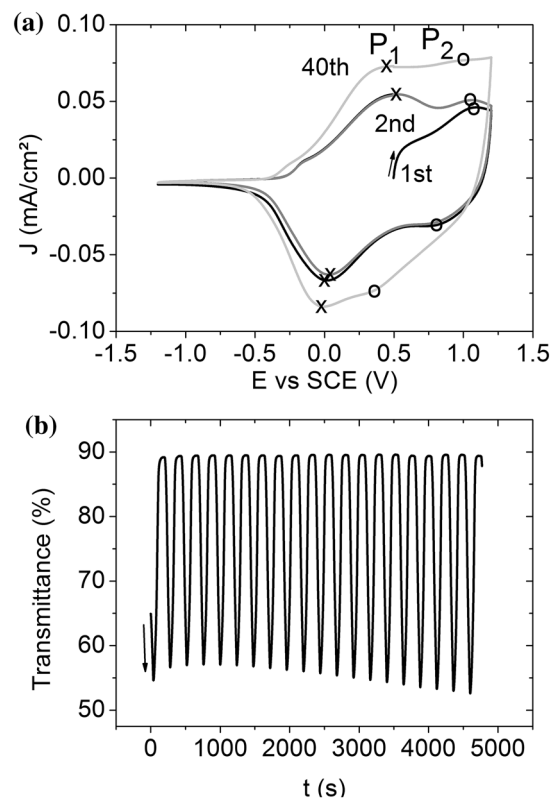


Fig. 6 CVs for 2 % $Ni_{1-x}O$ thin films cycled in Pt/0.3 M LiTFSI in BMITFSI/ $Ni_{1-x}O$ versus SCE, start in oxidation using a scan rate of 20 mV/s and -1.2 to 1.2 V voltage window (a). In situ measurement of transmittance during chronoamperometry operate at -1.2 V(20 s)/1.2 V(20 s) (b)

3.2 EC devices

In a final step, an ECD was built, from the association of WO_3 and 2 %- $Ni_{1-x}O$ thin films [8, 27], using a hydrophobic electrolyte membrane based on 0.3 M LiTFSI BMITFSI in PMMA (Solvionic) as ion conductor. Thickness of 200 nm for WO_3 and 250 nm for 2 %- $Ni_{1-x}O$ thin film were chosen in order to properly balance the capacities recorded in ionic liquid using three-electrode cell configuration. The transparent viscous mixture of ionic liquid in 40 % in PMMA was spread under ambient atmosphere on the WO_3 and 2 %- $Ni_{1-x}O$ electrochromic layers using a syringe and dried for 2 h at 80 °C under vacuum (~ 100 Pa.) to remove butanone leading to hydrophobic, sticky lithium conducting electrolyte membranes. Prior to device assembly, WO_3 thin film was cycled in 0.3 M LiTFSI BMITFSI electrolyte for few cycles and assembled in the bleached state of NiO counter electrode.

The shape of the cyclic voltammograms of the WO_3 /0.3 M LiTFSI BMITFSI in PMMA/2 %- $Ni_{1-x}O$ illustrates a well reversible behavior with good cyclability associated

with a capacity of 4.2 mC/cm^2 (Fig. 7). The optical transmittance carried out in situ with CAs, in which successively a potential of -2 V and one of $+0.1 \text{ V}$ were applied for 20 s , shows a modulation of the transmittance from 91 to 54% , corresponding to a contrast of 1.7 . A good stability was observed during 400 cycles (Fig. 8). These performances allow to calculate a coloration efficiency of $53 \text{ cm}^2/\text{C}$.

The evolution of the EC performances in respect of high (100°C) or low temperature (-35°C) remains poorly discussed in the literature while it is a critical issue for some of the applications [28, 29]. In our group, the influence of an increase in temperature or a decrease was investigated on WO_3/NiO devices (Fig. 9). The increase in cycling temperature leads to an increase in capacity, probably due to a slight increase in ionic conductivity of the electrolyte while the opposite behavior (decrease in capacity) is recorded for decreasing temperature. Indeed, at 35°C , the capacity becomes very low ($Q_{-35^\circ\text{C}} \approx 0.32 \text{ mC/cm}^2 \ll Q_{\text{RT}} \approx 2.5 \text{ mC/cm}^2 < Q_{60^\circ\text{C}} \approx 3.8 \text{ mC/cm}^2$). Interestingly, intermediate cycles at RT are not affected by previous cycling behavior at low temperature (Fig. 9a, b), as they regain similar capacities.

Despite the poor electrochemical capacity when cycled at low temperature, EC device still show some optical modulation determined using the chromaticity parameters. Table 3 gathers the colorimetric parameters in the CIE $L^*a^*b^*$ colorimetric space, recorded at -1.2 and 1.2 V at each temperature. The combination of $L^*a^*b^*$ parameters shows that the gray/neutral color hope for commercial purposes is obtained. The difference between bleached and colored state is essentially due to the L^* (luminescence) parameter. The parameter b^* seems to be slightly sensitive to the temperature and increases overall when the temperature decreases.

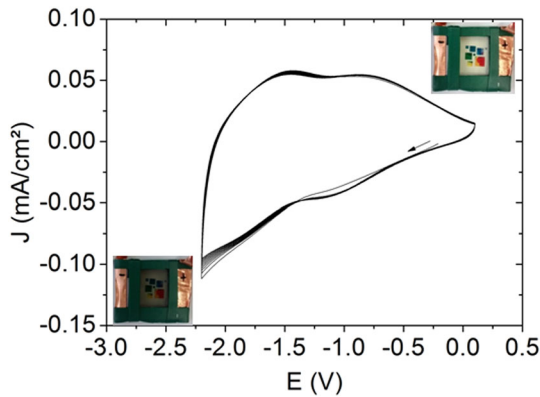


Fig. 7 CV of EC device $\text{WO}_3/0.3 \text{ M LiTFSI BMITFSI}$, $40\% \text{ PMMA}/2\% \text{ Ni}_{1-x}\text{O}$. The visual appearances of the device in the bleached and colored states are also added

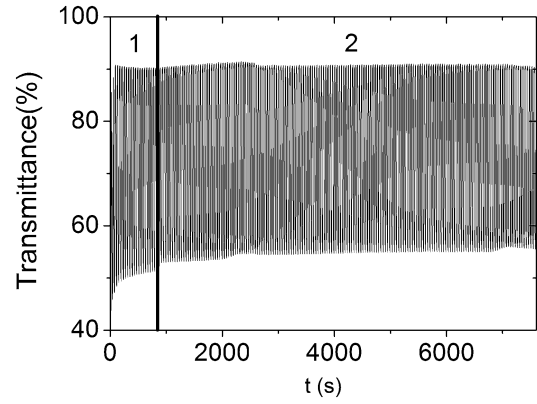


Fig. 8 Chronoamperometry of EC device $\text{WO}_3/0.3 \text{ M LiTFSI BMITFSI}$, $40\% \text{ PMMA}/2\% \text{ Ni}_{1-x}\text{O}$. Bleaching and coloration potentials are applied for 20 s each, at 0.1 V and 2.2 V in (1) and at 0.1 V and 2.0 V in (2)

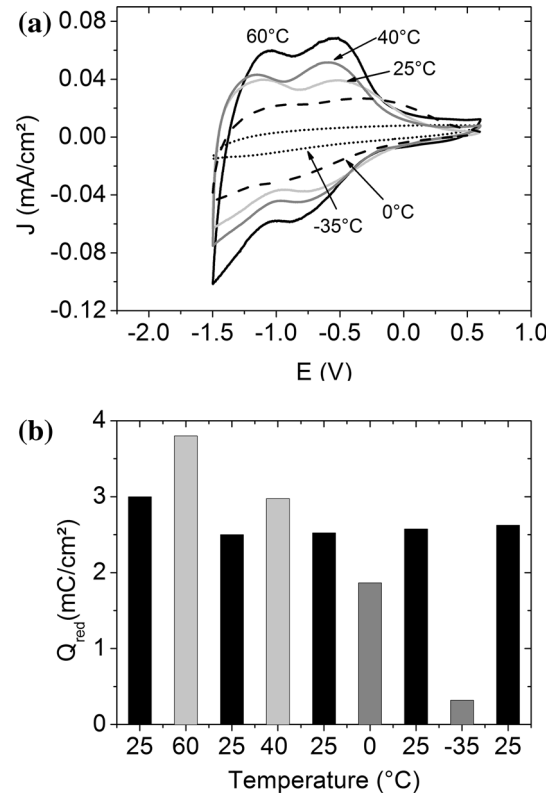


Fig. 9 CV of EC device $\text{WO}_3/0.3 \text{ M LiTFSI BMITFSI}$, $40\% \text{ PMMA}/2\% \text{ Ni}_{1-x}\text{O}$ at various temperatures (a) and histograms of the capacity versus temperature (b)

4 Conclusion

Non-stoichiometric NiO thin films were grown at RT using radio-frequency magnetron sputtering. Under increasing oxygen partial pressure from 0 to 10% of $\text{P}(\text{O}_2/\text{Ar} + \text{O}_2)$, well-crystallized thin films evolve from cubic Ni to cubic NiO structure. The optical properties of as-deposited films

Table 3 $L^*a^*b^*$ parameter of EC device $\text{WO}_3/0.3 \text{ M LiTFSI BMITFSI}$, 40 % PMMA/2 % Ni_{1-x}O at various cycling temperatures

	25 °C		60 °C		40 °C		0 °C		35 °C	
	Col	Bl	Col	Bl	Col	Bl	Col	Bl	Col	Bl
L^*	61.55	79.88	62.61	78.35	65.56	81.63	61.70	82.40	68.84	81.94
a^*	4.55	4.94	4.54	5.22	4.37	4.58	4.55	4.58	4.65	4.38
b^*	5.65	4.31	5.85	5.09	4.45	2.84	0.79	1.88	3.88	2.21

from reflective to transparent and brownish coloration illustrate an increase in the average nickel valence state. Cyclic voltammetry combined with in situ optical transmittance demonstrates an electrochemical process more complex than the only insertion/deinsertion of Li^+ , involving surface phenomena and in particular the contribution of anions (i.e., TFSI^-). The full device, $\text{WO}_3/0.3 \text{ M LiTFSI BMITFSI}$, 40 % PMMA/2 % Ni_{1-x}O , shows nice coloration efficiency of $53 \text{ cm}^2/\text{C}$ at room temperature. Cycling in temperature reveals an expected increase in capacity with increasing temperature while at -35°C , the capacity is very low. Surprisingly, whatever the temperature, the neutral/gray color resulting from the combination of WO_3 and NiO appears in the colored state. Those results emphasize the importance of the stoichiometry on the EC properties of nickel oxide thin films and that insertion/deinsertion mechanisms are no more the only ones to be considered.

Acknowledgments The authors wish to thank the University of Bordeaux for funding this research and in particular the Ph. D. grant of M. Da Rocha. The authors thank D. Michau, L. Teule Gay, S. Buffière and A. Fargues from ICMCB for their great help in experimental achievements and helpful discussions as well as A. Barnabé from CIRIMAT for electrical properties measurements.

References

1. C.G. Granqvist, *Handbook of Inorganic Electrochromic Materials* (Elsevier, Amsterdam, 1995)
2. E.L. Runnerstrom, A. Llordés, S. Lounis, D.J. Milliron, *Chem. Commun.* **50**, 10555 (2014)
3. J. Kim, G.K. Ong, Y. Wang, G. Leblanc, T.E. Williams, T.M. Mattox, B.A. Helms, D.J. Milliron, *Nanoletters* **15**, 5574 (2015)
4. C.M. Lampert, *Sol. Energy Mater.* **11**, 1 (1984)
5. S.K. Deb, *Sol. Energy Mater. Sol. Cells* **92**, 245 (2008)
6. J. Wang, E. Khoo, P.S. Lee, J. Ma, *J. Phys. C* **113**, 9655 (2009)
7. E. Washizu, A. Yamamoto, Y. Abe, M. Kawamura, K. Sasaki, *Solid State Ion.* **165**, 175 (2003)
8. J. Zhang, J.P. Tu, X.H. Xia, Y. Qiao, Y. Lu, *Sol. Energy Mater. Sol. Cells* **93**, 1840 (2009)
9. C. Marcel, J. M. Tarascon, *Solid State Ion.* **143**, 89 (2001)
10. C. Brigouleix, P. Topart, E. Bruneton, G. Campet, *Electrochim. Acta* **46**, 1931 (2001)
11. J. H. Choy, Y. L. Kim, B. W. Kim, G. Campet, J. C. Grenier, *Chem. Mater.* **12**, 2950 (2000)
12. D.S. Dalavi, E.S. Devan, R.A. Patil, J.H. Kim, P.S. Patil, *J. Mater. Chem. C* **1**, 3722 (2013)
13. A. Danine, L. Cojocaru, C. Faure, C. Olivier, T. Toupance, G. Campet, A. Rougier, *Electrochim. Acta* **129**, 113 (2014)
14. G.A. Niklasson, C.G. Granqvist, *J. Mater. Chem.* **17**, 127 (2007)
15. A. Surca, B. Orel, B. Pilhar, P. Bukovec, *J. Electroanal. Chem.* **408**, 83 (1996)
16. N. Penin, A. Rougier, L. Laffont, P. Poizot, J. M. Tarascon, *Sol. Energy Mater. Sol. Cells* **90**, 422 (2006)
17. D. Gillaspie, A. Norman, C.E. Tracy, S. H. Lee, A. Dillon, *J. Electrochem. Soc.* **157**, H328 (2010)
18. S. Pereira, A. Gonçalves, N. Correia, R. Martins, E. Fortunato, *Sol. Energy Mater. Sol. Cells* **120**, 109 (2014)
19. R. T. Wen, C.G. Granqvist, G.A. Niklasson, *Adv. Funct. Mater.* **25**, 3359 (2015)
20. E. Avendano, A. Azens, J. Isidorsson, R. Karmhag, G.A. Niklasson, C.G. Granqvist, *Solid State Ion.* **165**, 169 (2003)
21. S. Nandy, S. Biswajit, K. Mitra Manoj, K.K. Chattopadhyay, *J. Mater. Sci.* **42**, 5766 (2007)
22. F.F. Ferreira, M.H. Tabacniks, M.C.A. Fantini, I.C. Faria, A. Gorenstein, *Solid State Ion.* **86**, 88, 971 (1996)
23. M. Da Rocha, A. Rougier, *ECS Trans.* **66**, 1 (2015)
24. J. Denayer, G. Bister, F. Cambier, F. Cloots, *Appl. Surf. Sci.* **321**, 61 (2014)
25. M. Mihelcic, A. Surca Vuk, I. Jerman, B. Orel, F. Svegi, H. Moulki, C. Faure, G. Campet, A. Rougier, *Sol. Energy Mater. Sol. Cells* **120**, 116 (2014)
26. H. Moulki, C. Faure, M. Mihelcic, A. Surca Vuk, F. Svegl, B. Orel, G. Campet, M. Alfredsson, A.V. Chadwick, D. Gianolio, A. Rougier, *Thin Solid Films* **553**, 63 (2014)
27. S. Dulaud, A. Celik Cochet, I. Saadeddin, A. Labouret, G. Campet, G. Schottner, U. Posset, M. H. Delville, *New J. Chem.* **35**, 2314 (2011)
28. Y. Wei, J. Zhou, J. Zheng, C. Xu, *Electrochim. Acta* **166**, 277 (2015)
29. J.P. Matthews, J.M. Bell, I.L. Skryabin, *Electrochim. Acta* **44**, 3245 (1999)